ORGANOMETALLICS
Article
pubs.acs.org/Organometallics

A Dual-Emissive Phosphine–Borane Lewis Pair with a U-Shaped Linker: Impact of Methylation and Complexation on Fluoride Binding Affinity

Yufei Li,[†] Youngjin Kang,[‡] Jia-Sheng Lu,[†] Ian Wyman,[†] Soo-Byung Ko,[†] and Suning Wang*,[†]

[†]Department of Chemistry, Queen's University, Kingston, Ontario K7M 3N6, Canada
[‡]Division of Science Education, Kangwon National University, Chuncheon 200-701, Republic of Korea

Ⓢ *Supporting Information*

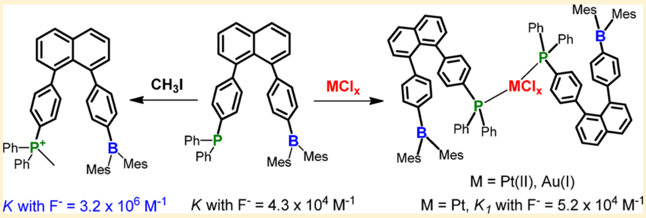

ABSTRACT: To investigate phosphine to borane through-space charge transfer and its utility in anion sensing and the formation of metal complexes, a phosphine–borane Lewis pair (**1**) connected by a U-shaped linker has been synthesized. **1** could be readily converted to a phosphonium salt (**2**) and two 2:1 complexes with Au(I) (**1-Au**) and Pt(II) (**1-Pt**). The photophysical properties of the new compounds were examined and compared. Compound **1** displayed an intense P → B CT transition and a bright solvent-dependent dual emission that is switchable by fluoride ions. **2** and **1-Pt** showed a turn-off and a turn-on fluorescent response, respectively, toward fluoride ions. The binding constant of **2** with F$^-$ was found to be 2 orders of magnitude greater than that of **1**. The mechanism that is responsible for the distinct fluorescence response of **1**, **2**, and **1-Pt** toward fluoride ions is proposed.

■ INTRODUCTION

Donor–acceptor compounds that contain a triarylboryl group are known to display charge transfer (CT) transitions, which can lead to bright fluorescence if connected by a conjugated linker[1] or weak fluorescence by a nonconjugated linker.[2a−c] Such donor–acceptor compounds have found broad applications in optoelectronic materials and sensory materials.[1,2] Nonconjugated donor–acceptor compounds are particularly interesting because they can faciliate turn-on fluorescent sensing for anions[2a−c] and may possess unusual reactivity as frustrated Lewis pairs.[3] Previously known nonconjugated donor–acceptor systems that display through-space CT fluorescence are limited to amino–borane compounds.[2a−c] Recently a number of nonconjugated phosphine–borane compounds incorporating P and B atoms that are directly attached to a 1,8-naphthyl backbone have been reported.[4] However, because the P and B atoms in these systems are bound to each other or are in very close proximity (P–B distance 2.08–3.05 Å), they show few interesting photophysical or chemical properties.[4] To force the P and B atoms apart and achieve through-space CT fluorescence, one effective approach is to insert a linker between the naphthyl and the P and B atoms. Such systems would allow us to access not only new through-space CT systems for sensing applications but also unusual reactivity introduced by the phosphine group, which is much more reactive than the conjugated amino group, and the bulky Lewis acidic boryl group in the vicinity.[3] On the basis of these considerations, we have obtained the first example of a U-shaped molecule, **1** (Scheme 1), which contains an unbound phosphine–borane pair and displays an intense dual emission with a distinct P → B CT emission peak and a strong switchable or "turn-on" response toward fluoride ions. Compound **1** can be readily converted to a phosphonium salt and metal complexes that display distinctively different response toward fluoride ions. The details are presented herein.

■ RESULTS AND DISCUSSION

Synthesis and Structures. Compound **1** was synthesized and isolated in overall 39% yield by the procedure shown in Scheme 1 via Negishi coupling of P(p-Br-Ph)Ph$_2$ with the BMes$_2$-phenyl functionalized iodo-naphthyl (**BI**), using Pd(PPh$_3$)$_4$ as the catalyst. Unlike the related N–B molecules with either an NMe$_2$ or an NAr$_2$ group, which do not bind to a metal ion and are very difficult to alkylate due to the stabilization of the lone pair via π conjugation with the aryl ring, the P–B compound **1** was readily methylated by reacting with CH$_3$I in a 1:1 ratio in refluxing THF, producing the phosphonium compound **2** in high yield.

Furthermore, despite the highly congested nature of molecule **1**, it could also bind readily to transition-metal ions, generating the metal complexes in high yields. The Au(I) complex (**1-Au**) and Pt(II) complex (**1-Pt**) were obtained by the reaction of **1** with Au(SMe$_2$)Cl and Pt(SMe$_2$)$_2$Cl$_2$, respectively, according to Scheme 2. Both complexes have a metal to ligand **1** ratio of 1:2. The 1:1 complex for the Au(I) metal ion was not observed when a 1:1 ratio of **1** and Au(SMe$_2$)Cl was used in the reaction. The metal complexes

Received: November 25, 2013

dx.doi.org/10.1021/om4011406 | *Organometallics* XXXX, XXX, XXX−XXX

Scheme 1. Synthetic Procedure for 1 and 2

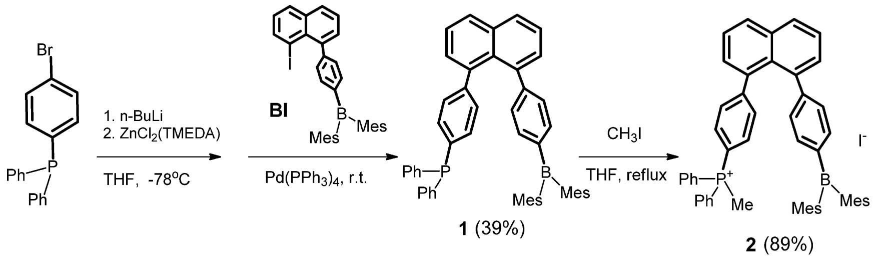

Scheme 2. Synthetic Procedure for 1-Au and 1-Pt

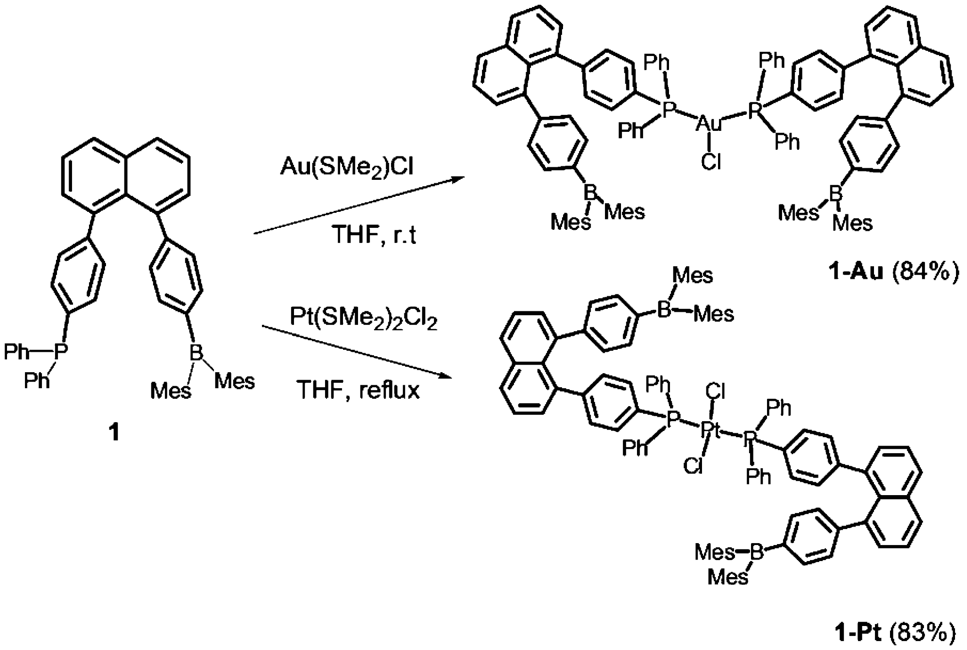

Table 1. Selected Bond Lengths (Å) and Angles (deg)

	bond length (Å)				
compound	B−C$_{Mes}$	B−C$_{Ph}$	P−C	M−Cl	M−P
1	1.575(4)	1.561(3)	1.831(2)		
	1.576(3)		1.832(3)		
			1.833(3)		
1-Au	1.59(1)	1.56(1)	1.819(7)	2.787(3)	2.319(2)
	1.59(1)		1.822(7)		
			1.826(7)		
1-Pt	1.551(9)	1.58(1)	1.811(6)	2.301(2)	2.316(2)
	1.57(1)		1.830(7)		
			1.851(8)		

	bond angle (deg)					
compound	C$_{Mes}$−B−C$_{Mes}$	C$_{Mes}$−B−C$_{Ph}$	C−P−C	P−M−Cl	P−M−P	Cl−M−Cl
1	118.9(2)	121.4(2)	103.4(1)			
		119.7(2)	100.6(1)			
			102.9(1)			
1-Au	124.0(7)	118.0(6)	101.6(3)	100.84(5)	158.31(9)	
		117.9(7)	104.3(3)			
			105.2(3)			
1-Pt	124.0(6)	117.5(6)	104.2(3)	94.34(7)	180.0	180.0
		118.5(6)	106.4(3)	85.66(7)		
			105.7(3)			

were fully characterized by NMR and elemental analyses. In the ^{31}P NMR spectra, compound **1** displays a characteristic phosphine signal at −6.0 ppm, while that of **2** appears at 22.4 ppm, as is typical of phosphonium.[5] For the metal complexes, the ^{31}P chemical shift appears at 33.5 ppm for **1-Au** and 19.5 ppm for **1-Pt**, indicating that the phosphine center donates electrons to the AuCl unit more effectively than the PtCl$_2$ unit.[6] To fully understand the properties of these new compounds, the crystal structures of **1**, **1-Au**, and **1-Pt** were determined by X-ray diffraction analysis. Efforts to grow single crystals of compound **2** were unsuccessful. The crystal structures of **1**, **1-Au**, and **1-Pt** are shown in Figures 1−3, respectively. Key bond lengths and angles are given in Table 1.

The P atom in **1** has a typical pyramidal geometry, while the B atom has a typical trigonal-planar geometry. Because of steric interactions, the two phenyl linkers are repelled by each other and the dihedral angles between the peri phenyls and the naphthyl benzene ring are significantly distorted from 90° (∼127°). The C−C bond lengths between the phenyl linkers and the naphthyl carbon atoms are 1.488(3) and 1.489(3) Å, respectively, which are typical of a C−C single bond. The separation distance between the B and the P atom is 6.24(1) Å, a distance that is much longer than those of the closely related N−B systems (∼5.5 Å)[2a−c] and can be attributed to the sterically demanding pyramidal geometry of the P unit. The naphthyl ring is also considerably distorted from planarity, as indicated by the 16.2° dihedral angle between the two fused benzene rings and the side view of the structure in Figure 1.

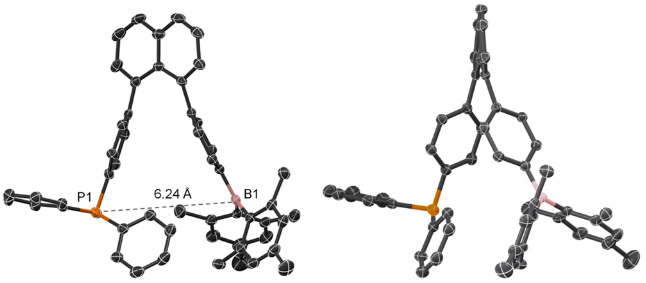

Figure 1. Diagrams showing the structure of **1** with 35% thermal ellipsoids: (left) front view; (right) side view. H atoms are omitted for clarity.

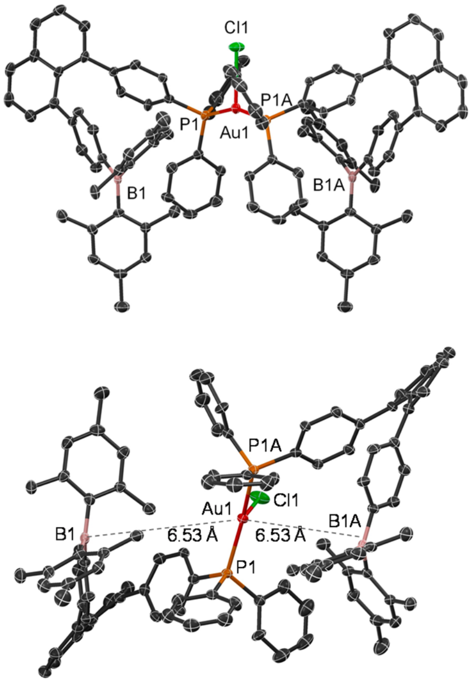

Figure 2. Diagrams showing the structure of **1-Au** with 35% thermal ellipsoids: (top) side view; (bottom) front view. H atoms are omitted for clarity.

The structure of **1-Au** compound is shown in Figure 2. This molecule has a crystallographically imposed C_2 symmetry with a helical arrangement of the two **1** ligands. The Au(1) atom has a triangular arrangement with the two B atoms (Au(1)···B(1) = 6.53 Å, B(1)···Au(1)···B(1A) = 122.0°). The Au(I) center is bound by two P atoms and one Cl anion with an approximate T shape, as evidenced by the P(1)−Au(1)−P(1A) angle (158.31(9)°) and the P(1)−Au(1)−Cl(1) angle (100.84(5)°). Although many examples of three-coordinate Au(I) compounds with a T-shaped geometry have been known previously,[7] the structure of **1-Au** is unusual. In comparison to the closely related compound Au(PPh$_3$)$_2$Cl, which has an approximate trigonal-planar geometry with a P−Au−P angle of 132.1(1)° and P−Au−Cl angles of 109.2(1) and 112.8(1)°,[7b] **1-Au** is much more distorted from a trigonal-planar geometry. Further, the Au(1)−P(1) bond length (2.319(2) Å) in **1-Au** is similar to those in Au(PPh$_3$)$_2$Cl (2.323(4), 2.339(4) Å), but the Au(1)−Cl(1) bond (2.787(3) Å) is much longer than that in Au(PPh$_3$)$_2$Cl (2.500(4) Å) and the sum of the covalent radii[8] of Au(I) and Cl$^-$ (2.33 Å). Thus, the Au(I) center in **1-Au** may be best described as a distorted-linear geometry with a weakly bound Cl$^-$. The significant departure of **1-Au** from the trigonal-planar geometry displayed by Au(PPh$_3$)$_2$Cl may be attributed to the steric bulkiness of the ligand **1**. In the crystal lattice, there are CHCl$_3$ solvent molecules (4 CHCl$_3$/per **1-Au**), two of which form H bonds with the Cl ion in **1-Au** (see the Supporting Information). Because of the steric congestion, no short Au···Au interactions are present in the lattice.

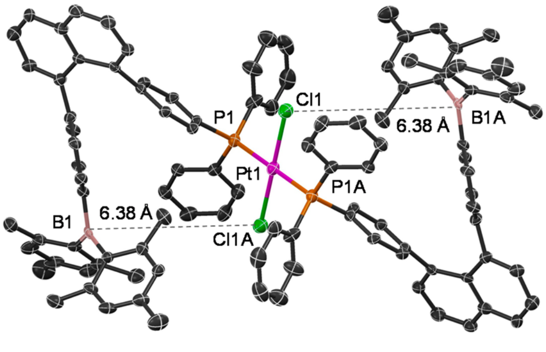

Figure 3. Diagrams showing the structure of **1-Pt** with 35% thermal ellipsoids. H atoms are omitted for clarity.

The structure of **1-Pt** is shown in Figure 3. Like the **1-Au** molecule, the Pt(II) center is also bound by two **1** ligands. The molecule of **1-Pt** has a crystallographically imposed inversion center with a trans square-planar geometry. Unlike **1-Au**, which has a very long Au−Cl bond, the Pt−P and Pt−Cl bond lengths are typical (Table 1). The higher coordination number and the much shorter Pt−Cl bonds in **1-Pt**, in comparison to those of **1-Au**, are consistent with the greater donation of the P atoms to the metal center in **1-Au**, as indicated by the ^{31}P NMR data. The Pt···B distance is very long at 7.31 Å. The chloride ions are oriented toward the B atom with a separation distance of 6.38 Å. In solution, the trans isomer was observed exclusively, which is clearly favored by the bulky ligand **1**. In the crystal lattice, the Pt(II) units of **1-Pt** are stacked along the *a* axis with a very long Pt···Pt separation distance (8.59 Å).

Absorption and Fluorescence Spectra. *Compound 1.* Compound **1** has an intense absorption band at λ_{max} 330 nm that does not change significantly with solvent polarity (see Table 2). In the fluorescence spectrum, **1** shows dual emission in most solvents except coordinating solvents such as DMSO, DMF, and CH_3CN, in which the fluorescence spectrum of **1** displays either only one emission peak at ~410 nm (DMSO, DMF) or is dominated by the 410 nm emission peak (CH_3CN) (see Figure 4 and the Supporting Information). The high-energy emission peak of **1** exhibits a small red shift (e.g., λ_{max} 400 nm in hexane and 415 nm in acetone) with increasing solvent polarity, while the low-energy signal shows a pronounced red shift (λ_{max} 460 nm in hexane and 554 nm in acetone). Because of the dual emission, **1** has a white fluorescence color in THF and CH_2Cl_2. The dual emissive behavior of **1** is in sharp contrast to the previously reported U-shaped amino–$BMes_2$ molecules with a similar 1,8-diphenylnaphthyl linker between an NMe_2 or an NAr_2 donor and a $BMes_2$ acceptor, which display the N → B CT emission peak only.[2] This difference can be explained by the stabilization of the amino radical cation through π conjugation with the aryl group that stabilizes the charge-separated excited state in the N–B compounds, making the CT emission an efficient and competitive relaxation pathway in the N–B compounds.

Table 2. Photophysical Properties[a]

		absorption		fluorescence[b]	
compound	solvent	λ_{max} (nm)	log ε	λ_{em} (nm)	Φ_{FL}
1	hexanes	330	4.53	400 (sh), 460	0.30
	toluene	335	4.45	404 (sh), 493	0.31
	CH_2Cl_2	330	4.50	407, 532	0.13
	THF	335	4.41	404, 530	0.04
	acetone	335	4.43	415, 554	0.07
	DMSO	335	4.40	422	0.25
2	CH_2Cl_2	340	4.48	410	0.55
1-Au	CH_2Cl_2	335	4.87	402	0.44
1-Pt	CH_2Cl_2	330	4.60	408	0.02

[a] All spectra were recorded using a 1.0×10^{-5} M solution. [b] The fluorescence quantum efficiency was determined using 9,10-diphenylanthracene as a reference.

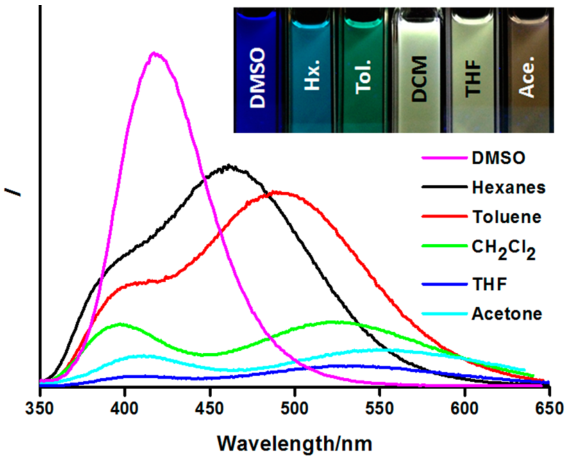

Figure 4. Fluorescence spectra and photographs showing the emission color of **1** in various solvents (λ_{ex} 330 nm, 1.0×10^{-5} M) with relative intensities. The fluorescence spectra in DMF and CH_3CN can be found in the Supporting Information.

On the basis of the solvent dependence of the dual emission and the previous study on the related N–B systems, the low-energy peak of **1** was assigned to a P → B through-space CT transition while the high-energy peak corresponds to a Mes (π) → B-Ph (π*) transition. This assignment was further supported by the fact that a diboron compound which has a structure similar to that of **1** except that the phosphine group in **1** is replaced with a $BMes_2$ displays the high-energy emission peak only.[2d] The abnormal behavior of **1** in DMSO, DMF, and CH_3CN was most likely caused by the weak coordination of these solvent molecules to the B center that blocks the P → B CT, since a similar phenomenon was observed in the previously reported U-shaped N–B molecules.[2] Thermal quenching of the CT emission may also be a factor due to the low energy of the CT state in the high-polarity solvents. The fluorescent quantum efficiency (Φ_{FL} = 0.07 in acetone, 0.13 in CH_2Cl_2, and 0.30 in hexane) of **1** increased with decreasing solvent polarity, as the P → B CT peak shifts toward higher energy.

The assignment of the dual emission in **1** was also supported by TD-DFT calculation data on the vertical excitation of the ground state (Table 3 and Figure 5). The S_1 transition of **1** is mainly the P lone pair (HOMO) → B-Ph (π*, LUMO) CT transition with significant contributions from the naphthyl to

Table 3. TD-DFT Calculated Vertical Excitation Energy and Oscillator Strengths for All Compounds and the Fluoride Adducts of 1 and 2

compound	state	transition	energy (nm)	oscillator strength $(f)^a$
1	S_1	H → L (80%)	362	0.2522
	S_2	H-2 → L (80%)	359	0.0806
2[b]	S_1	H → L (91%)	369	0.0113
	S_2	H → L+1 (70%)	361	0.0878
NMe_4[1-F]	S_1	H → L (99%)	417	0.0026
	S_3	H-2 → L (77%) H-3 → L (19%)	369	0.0490
	S_4	H-2 → L (21%) H-3 → L (76%)	358	0.1818
2-F	S_2	H → L+1 (98%)	409	0.0083
	S_4	H-2 → L (93%)	371	0.0024
1-Pt	S_4	H-4 → L (22%) H-3 → L+1 (39%)	369	0.0159
	S_5	H-4 → L+1 (33%) H-3 → L (25%)	368	0.1019
1-Au	S_1	H → L (93%)	436	0.0030
	S_3	H-1 → L+1 (93%)	399	0.0030
	S_7	H → L+3 (95%)	379	0.0040
	S_8	H → L+2 (92%) H-6 → L+1 (32%)	378	0.0030
	S_9	H-5 → L (33%) H-6 → L+1 (32%)	367	0.0112
	S_{10}	H-6 → L (32%) H-5 → L+1 (32%)	367	0.2075

[a] Vertical excitation states with f < 0.001 are not given. For the full listing, please see the Supporting Information. [b] The anion used in the computation for **2** is PF_6^-.

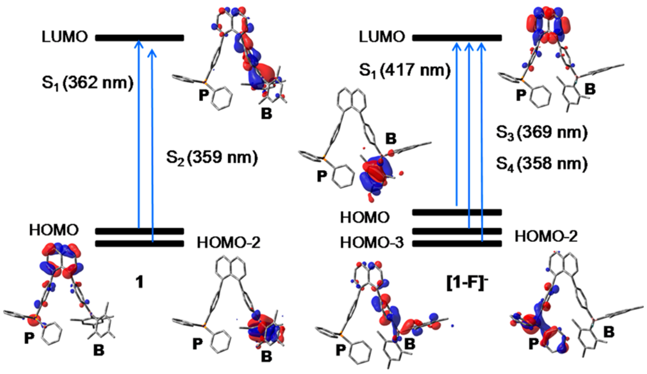

Figure 5. Electronic transitions and the associated MO diagrams that are responsible for the low-energy absorption bands of **1** and NMe$_4$[**1-F**]. The MO diagrams are plotted with an isocontour value of 0.03. The NMe$_4^+$ cation was omitted for clarity.

the HOMO and a great oscillator strength (f = 0.2522). The S$_2$ transition (HOMO-2 → LUMO, 80%) is mainly from the Mes (π) → B-Ph (π*) transition with a smaller oscillator strength (0.0806). The calculated vertical excitation energies of these two states are close. In solution, the S$_1$ state could be greatly stabilized by polar solvent molecules due to the highly polarized nature of this state, leading to the distinct solvent polarity dependent CT emission. Thus, the high-energy and low-energy emission peaks of **1** are mostly likely from the S$_2$ and S$_1$ states, respectively.

*Compounds **2**.* The absorption spectrum of **2** is red-shifted, in comparison to that of **1** (Figure 6). The fluorescence spectrum of **2** has only one emission peak at 410 nm in CH$_2$Cl$_2$ that is red-shifted by a few nanometers, in comparison to that of **1** (Figure 7). The absence of the low-energy emission peak in the spectrum of **2** further confirmed that the low-energy peak of **1** is indeed from a P → B CT transition, since such a transition is not possible in **2**. The fluorescent quantum efficiency (0.55 in CH$_2$Cl$_2$) of **2** is much higher than that of **1** (0.13).

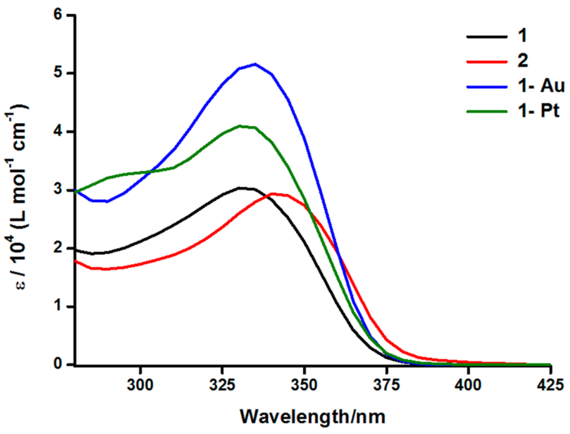

Figure 6. Absorption spectra of **1**, **2**, **1-Au**, and **1-Pt** in CH$_2$Cl$_2$.

TD-DFT computational results for **2** indicated that the S$_1$ transition is mainly from a HOMO → LUMO transition (91%, oscillator strength 0.0113) and is 7 nm lower in energy than that of **1**, while the S$_2$ transition that is close in energy is dominated by a HOMO → LUMO+1 transition (70%, oscillator strength 0.0878). As shown in Figure 8, the HOMO and LUMO levels of **2** are localized on the mesityl ring and the phosphonium unit, respectively, while LUMO+1 is mainly on the phenyl linker between the phosphonium and the naphthyl with a significant contribution from the empty p orbital of the boron atom. The fluorescence of **2** may be therefore attributed to a mixed transition of Mes(π) → phosphonium(π*) and Mes(π) → Ph(π*).

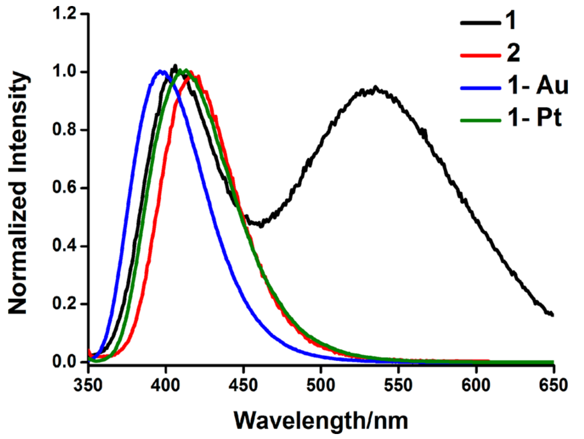

Figure 7. Normalized fluorescent emission spectra of **1**, **2**, **1-Au**, and **1-Pt** in CH$_2$Cl$_2$.

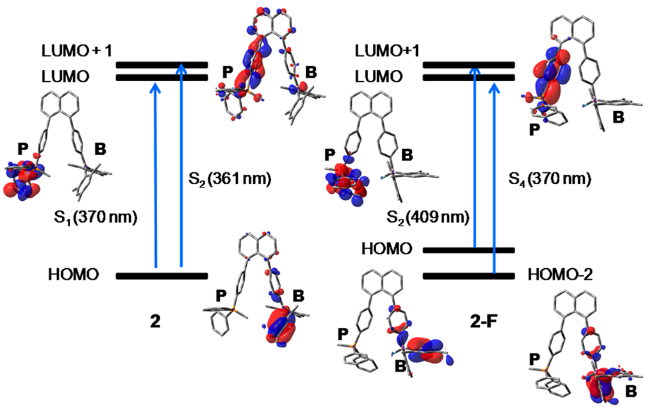

Figure 8. Electronic transitions and the associated MO diagrams that are likely responsible for the low-energy absorption bands of **2** and **2-F**. The MOs are plotted with an isocontour value of 0.03. The PF$_6^-$ anion in **2** is omitted for clarity.

Metal Complexes. The absorption spectra of the metal complexes are similar to that of **1** (Figure 6). No phosphorescence was observed for **1-Au** and **1-Pt** even at 77 K. The fluorescence spectra of **1-Au** and **1-Pt** resemble that of **2** with λ_{max} at 402 and 408 nm, respectively (Figure 7), consistent with the blocking of the P → B CT transition by metal ion coordination. Surprisingly, the Φ_{FL} value (0.44 in CH$_2$Cl$_2$) of **1-Au** is much higher than that of **1**, but that of **1-Pt** is much lower (0.02 in CH$_2$Cl$_2$).

TD-DFT data showed that for **1-Pt** the S$_1$–S$_3$ states all have an oscillator strength of 0.000 involving mostly the transition of the Cl$^-$ lone pair electrons and the Pt(II) d electrons to a Pt–ligand (Cl and C) σ* orbital (n → σ*); thus, they are unlikely to be responsible for the observed fluorescence. The S$_4$ and the S$_5$ states of **1-Pt** are degenerate with an appreciable oscillator strength, involving transitions of HOMO-3/HOMO-4 to LUMO/LUMO+1 (57–61%) that may be described as Mes(π) → B-Ph(π*) transitions, similar to the S$_2$ state of **1** and **2**, as shown in Figure 9. The fluorescence of **1-Pt** is therefore most

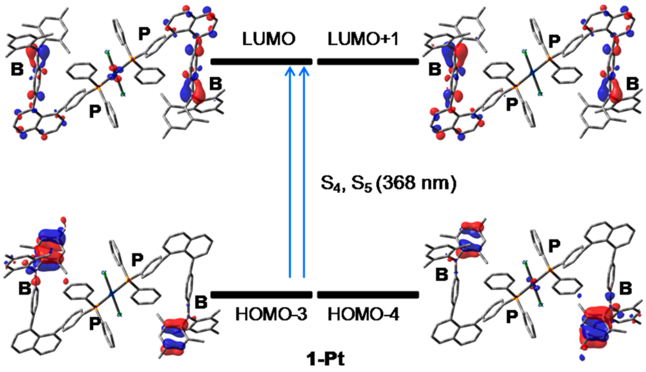

Figure 9. Electronic transitions and the associated MO diagrams that are likely responsible for the low-energy absorption bands of **1-Pt**. The MOs are plotted with an isocontour value of 0.03.

likely from these transitions. For the **1-Au** compound, TD-DFT data indicated that the S_1−S_8 states all have either a 0 or a very small oscillator strength (<0.004) involving transitions mostly from the lone pairs of the chloride ion to the B-Ph π* orbitals (Cl^- → π*) (see the Supporting Information). They are therefore not likely to be responsible for the bright fluorescence of **1-Au**. Similar to those observed in **1-Pt**, the S_9 and S_{10} transitions in **1-Au** are degenerate, involving HOMO-5/HOMO-6 to LUMO/LUMO+1 (64−65%) transitions, and may be ascribed as Mes(π) → B-Ph(π*) transitions, as shown in Figure 10. Furthermore, the vertical excitation energies of S_9 and S_{10} in **1-Au** are similar to those of S_4 and S_5 in **1-Pt**. We therefore suggest that the fluorescence of **1-Au** likely has the same origin as that of **1-Pt**: namely, the Mes(π) → B-Ph(π*) transition. The low fluorescent Φ_{FL} value of **1-Pt** is likely caused by partial quenching of the Mes(π) → B-Ph(π*) transition by the low-lying n → σ* states. Similar quenching in **1-Au** by the low-lying Cl^- → π* states is likely to a much lesser degree due to the weak association of the chloride ion with the complex, as indicated by the very long Au−Cl bond in the crystal structure, which is very likely fully dissociated in solution, giving the propensity of the Au(I) ion to adapt a linear two-coordinate structure.

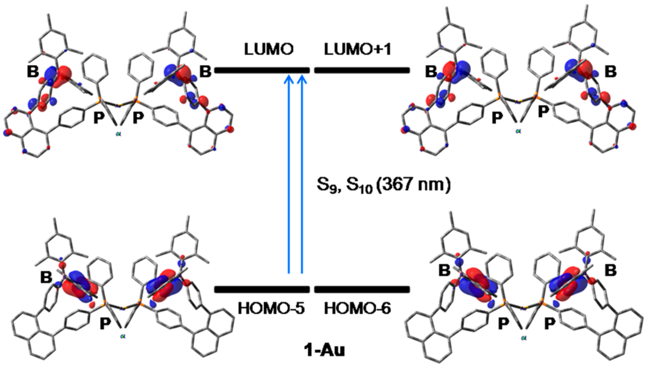

Figure 10. Electronic transitions and the associated MO diagrams that are likely responsible for the low-energy absorption bands of **1-Au**. The MOs are plotted with an isocontour value of 0.03.

Fluoride Sensing. Fluoride titration experiments for **1**, **2**, and **1-Pt** were performed. **1-Au** was not investigated for fluoride sensing, because the loosely bound chloride ion on the Au center can be readily replaced by a fluoride ion and complicates the matter. The response of **1**, **2**, and **1-Pt** toward fluoride ions was examined in both absorption and fluorescence modes.

In the absorption spectra, the addition of fluoride ions caused a substantial intensity increase of the 330 nm peak for **1** (Figure 11). In the fluorescence spectrum, the addition of fluoride ions led to quenching of the low-energy CT peak and enhancement of the high-energy emission peak of **1**, with Φ_{FL} increasing from 0.13 to 0.29 and an emission color change from whitish yellow to deep blue, as shown in Figure 11. This response could be ascribed as a "turn-on" or "switchable" fluorescence sensing, a phenomenon similar to that observed in the related N−B compounds, although the high-energy emission peak only appears after the addition of fluoride ions in the N−B compounds.[2b,c] The more than doubled fluorescent quantum efficiency of **1** after the addition of fluoride ions is in sharp contrast to the case for the related N−B compounds,[2b,c] which have either a small increase or no increase at all in fluorescent quantum efficiency with fluoride addition, making **1** more sensitive as a ratiometric probe for fluoride ions than the related N−B compounds. Indeed, ~2 equiv of F^- was needed to reach the saturation point for **1**, while more than 20 equiv of F^- was needed to achieve the same effect for the related N−B compounds.[2b,c] The large emission energy difference between the P → B CT peak in **1** and the fluorescent peak in $[\mathbf{1\text{-}F}]^-$ in comparison to that for the related N−B compounds may be partially responsible for the great quantum efficiency increase. The increase of the absorbance of the excitation band at 330 nm with fluoride addition, as shown in Figure 11, was clearly a

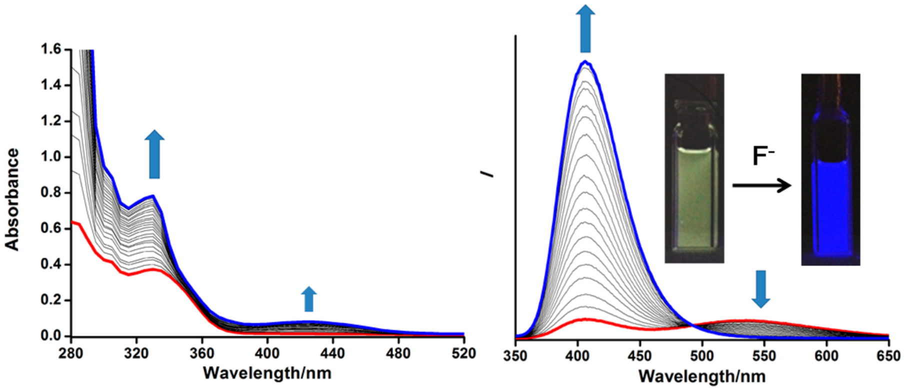

Figure 11. Absorption (left) and fluorescence (right) spectral changes of **1** in CH_2Cl_2 upon the addition of NBu_4F. The fluorescence spectrum was recorded using 330 nm excitation.

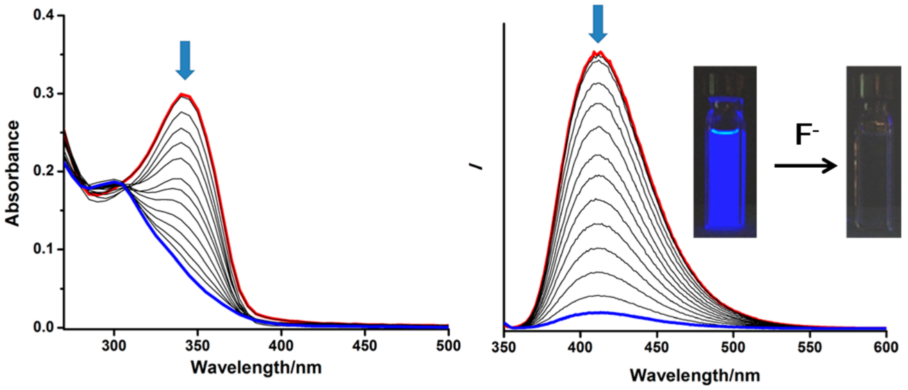

Figure 12. Absorption (left) and fluorescence (right) spectral changes of **2** in CH_2Cl_2 upon the addition of NBu_4F. The fluorescence spectrum was recorded using 340 nm excitation.

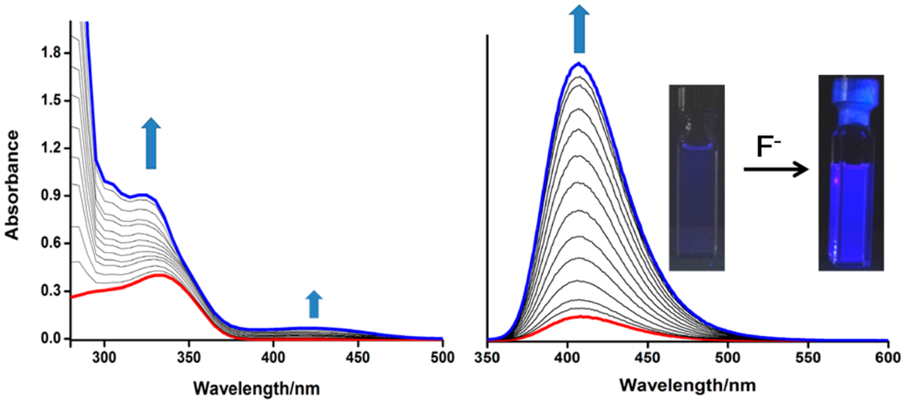

Figure 13. Absorption (left) and fluorescence (right) spectral changes of **1-Pt** in CH_2Cl_2 upon the addition of NBu_4F. The fluorescence spectrum was recorded using 330 nm excitation.

key factor for the enhancement of the high-energy emission peak in **1**. The quenching of the CT band was clearly caused by the blocking of the empty p orbital of the B center by the fluoride ion. The binding of fluoride to the B center in **1** was confirmed by the characteristic four-coordinate ^{11}B chemical shift (3.8 ppm) observed for [**1-F**]$^-$ and the ^{19}F chemical shift (−175.7 ppm; see the Supporting Information), typical for fluoride ions bound to a $BMes_2Ar$ unit.[2]

As shown by the TD-DFT data in Table 3 and Figure 5, the S_1 state of the fluoride adduct [**1-F**]$^-$ is lower in energy than that of **1** and involves the transition from the $BFMes_2$ unit (HOMO) to the naphthyl π^* (LUMO) with a very weak oscillator strength (0.0026). This is in agreement with the appearance of a very weak absorption band at about 430 nm in the absorption spectrum of NBu_4[**1-F**] (Figure 11). The fact that [**1-F**]$^-$ is nonemissive on excitation at 430 nm supports that the fluorescence of [**1-F**]$^-$ is not from the S_1 state. Therefore, we suggest that the fluorescence of [**1-F**]$^-$ is likely from the S_3 or the S_4 state that involves a transition from either the $BFMes_2$-Ph (π, HOMO-2) or the PPh_2-Ph (π, HOMO-3) to the naphthyl (π^*, LUMO), which happens to have a energy similar to that of the S_2 state of **1**.

In contrast to **1**, the addition of fluoride ions to **2** caused partial quenching of the 340 nm peak in the absorption spectrum and the emission peak at 410 nm in the fluorescence of **2** with a Φ_{FL} change from 0.55 to 0.06 and the disappearance of the deep blue emission color (Figure 12). Clearly the decrease of absorbance at 340 nm—the excitation energy used—was responsible for the decrease of the emission peak and the emission quantum efficiency. The binding of fluoride to the B center in **2** was also confirmed by the ^{11}B chemical shift (3.5 ppm) observed for [**2-F**] and the ^{19}F chemical shift (−167.7 ppm; see the Supporting Information) that are similar to those observed for [**1-F**]$^-$.

TD-DFT data showed that the S_1−S_{15} states in **2-F** all have either 0.000 or very weak oscillator strengths (Table 3), which is in agreement with the observed quenching in absorption and fluorescence spectra of **2** upon the addition of fluoride ions. The first two excited states S_2 and S_4 in **2-F** that have appreciable oscillator strengths are shown in Figure 8 and Table 3.

For **1-Pt**, the addition of fluoride ions enhanced the absorption band at 330 nm and the fluorescence peak at 408 nm with a Φ_{FL} increase from 0.02 to 0.10, in a manner similar to that observed for **1** (Figure 13). The increase of the fluorescence intensity in the fluoride adduct of **1-Pt** was attributed to the increase of absorbance of the excitation band. A low-energy absorption band at ~425 nm was observed for the fluoride adduct of **1-Pt**, which likely shares the same origin as that of [**1-F**]$^-$ ($BFMes_2$ → naphthyl). Although TD-DFT calculations were not performed for the fluoride adduct of **1-Pt** due to the large size of the molecule, on the basis of the similarity of the absorption and fluoreescence profiles and energies, we suggest that the fluorescence of the fluoride adduct of **1-Pt** is likely from the state of $BFMes_2$-Ph → naphthyl, similar to that observed in [**1-F**]$^-$.

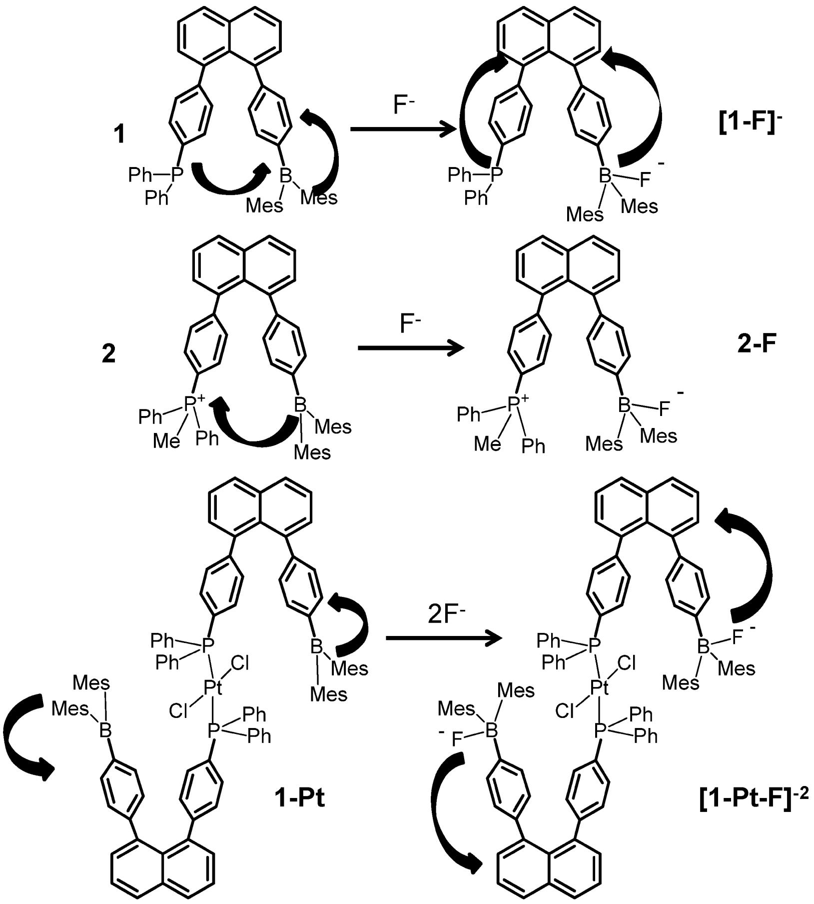

Figure 14. Proposed fluorescence change mechanism of **1**, **2**, and **1-Pt** upon the addition of fluoride ions. The arrows indicate the charge transfer states that are likely responsible for the fluorescence of these molecules.

The impact of fluoride on fluorescence and the possible origin of fluorescence for **1**, **2**, and **1-Pt** and their fluoride adducts are illustrated in Figure 14.

To examine the effect of the Coulombic force on the fluoride binding strength of the borane center in **2**, the binding constants of **1** and **2** with F^- were determined and compared. The binding constant of **1** ($(4.3 \pm 0.5) \times 10^4$ M^{-1}) was found to be greater than that of a closely related N—B compound ($(1.6 \pm 0.5) \times 10^4$ M^{-1}),[2c] while the binding constant of **2** with F^- ($(3.2 \pm 1.0) \times 10^6$ M^{-1}) was found to be about 100 times greater than that of **1** (see the Supporting Information). The large binding constant increase from **1** to **2** can be attributed to the Coulombic attraction exerted by the phosphonium ion, despite its long distance from the borane group. Combining Coulombic interactions with a borane center by attaching a peripheral cationic group such as a phosphonium has been demonstrated previously to be highly effective in enhancing the binding strengh of F^- to the sensor by Gabbaï and others.[5,9] The K_1 and K_2 binding constants of **1-Pt** with F^- were found to be $(5.2 \pm 1.0) \times 10^4$ and $(7.9 \pm 2.0) \times 10^3$ M^{-1}, respectively (see the Supporting Information), indicating that the attachment of a neutral metal unit to the phosphine center in the U-shaped molecule **1** has little influence on the sensitivity of the borane center toward fluoride ions, perhaps due to the greatly increased steric congestion and the long separation distance between the metal and the boron atom.

■ CONCLUSIONS

In summary, an unbound phosphine—borane compound that displays a distinct through-space CT transition and intense dual emission has been obtained. The use of the new P—B compound in turn-on/switchable fluorescent sensing of fluoride has been demonstrated. The P—B compound was found to have a ratiometric response toward fluoride ions greater than that of the related N—B compounds. Converting the P—B compound to its phosphonium salt was found to greatly enhance the binding affinity of the borane center toward fluoride ions by 2 orders of magnitude. Despite the great steric congestion, the new P—B molecule was found to be an effective ligand for metal ions such as Au(I) and Pt(II). The utility of the new P—B molecule as a bulky and bifunctional ligand in enhancing the chemical reactivity of transition-metal complexes is currently being examined, and the results will be reported in due course.

■ EXPERIMENTAL SECTION

General Procedures. All reactions were carried out under a nitrogen atmosphere. Reagents were purchased from Aldrich Chemical Co. and used without further purification. Thin-layer and flash chromatography were performed on silica gel. ^1H, ^{13}C and ^{31}P NMR spectra were recorded on Bruker Avance 400 and 500 MHz spectrometers. Deuterated solvents were purchased from Cambridge Isotopes. UV—vis spectra were recorded on a Varian Cary 50 UV—visible spectrophotometer. Emission spectra were recorded using a Photon Technologies International QuantaMaster Model 2 spectrometer. Fluorescent quantum yields were determined using optically dilute solutions ($A \approx 0.1$) relative to 9,10-diphenylanthracene ($\Phi = 0.90$). Fluorescence titrations were carried out by adding stock solutions of TBAF in CH_2Cl_2 to the solutions of **1**, **2**, and **1-Pt** in CH_2Cl_2. The starting material **BI** was prepared using a modified literature procedure.[2]

Synthesis of 1. 1-(Diphenylphosphino)-4-bromobenzene (316 mg, 0.926 mmol) was dissolved in 20 mL of dry degassed THF in a 50 mL Schlenk flask with a stir bar. After the solution was cooled to −78 °C for 15 min, *n*-BuLi (0.64 mL, 1.6 M in hexanes, 1.020 mmol) was added dropwise. The mixture was stirred 1 h at −78 °C. $ZnCl_2$(TMEDA) (292 mg, 1.158 mmol) was added. The mixture was warmed to room temperature slowly and stirred for 1 h. **BI** (359 mg, 0.620 mmol) and $Pd(PPh_3)_4$ (80 mg, 0.069 mmol) were added, and the reaction mixture was stirred and refluxed for 40 h. After the removal of the solvent in vacuo, the residue was partitioned between CH_2Cl_2 and water and the aqueous layer was extracted twice with CH_2Cl_2. The combined organic layers were dried over $MgSO_4$ and filtered. Purification on a silica gel column (5/1 hexanes/CH_2Cl_2 as eluent) afforded 257 mg of **1** as a white solid (39% yield). ^{1}H NMR (500 MHz, CD_2Cl_2, δ): 7.98 (d, $^3J_{H-H}$ = 7.88 Hz, naph, 2H), 7.61 (m, naph, 2H), 7.43 (t, $^3J_{H-H}$ = 5.6 Hz, naph, 2H), 7.26 (m, Ph, 12H), 7.10 (t, $^3J_{H-H}$ = 7.0 Hz, Ph, 4H), 7.01 (t, $^3J_{H-H}$ = 6.94 Hz, Ph, 2H), 6.88 (s, Mes, 4H), 2.36 (s, Me, 6H), 2.03 (s, Me, 12H) ppm. ^{31}P{^{1}H} NMR (202 MHz, CD_2Cl_2, δ): −6.0 ppm. ^{11}B{^{1}H} NMR (160 MHz, C_6D_6, 70 °C, δ): 74.3 ppm. ^{13}C NMR (126 MHz, CD_2Cl_2, δ): 148.4 (Ph), 144.6 (naph), 142.1 (Mes), 141.4 (Mes), 140.6 (d, Ph, J_{C-P} = 29.3 Hz), 138.9 (Mes), 138.2 (d, Ph, J_{C-P} = 12 Hz), 137.3 (ph), 136.2 (Ph), 134.0 (d, Ph, J_{C-P} = 19.5 Hz), 133.5 (d, Ph, J_{C-P} = 19.4 Hz), 131.9 (Ph), 131.7 (naph), 130.1 (Ph), 129.7 (Ph), 129.0 (naph), 128.9 (naph), 128.7 (Mes), 125.8 (d, Ph, J_{C-P} = 11 Hz), 24.4 (Me), 21.5 (Me) ppm. Anal. Calcd for $C_{52}H_{46}BP$: C, 87.60; H, 6.40. Found: C, 87.72; H, 6.56.

Synthesis of 2. Compound **1** (50 mg, 0.07 mmol) was dissolved in 10 mL of dry and degassed THF. Iodomethane (4.4 μL, 0.07 mmol) was added to the solution dropwise. The mixture was stirred and refluxed overnight. After the solvent was removed in vacuo and 5 mL of hexanes was added, a precipitate was obtained and washed with diethyl ether to afford 53 mg of **2** as a colorless solid (89% yield). Compound **2** was recrystallized from CH_2Cl_2/hexane. ^{1}H NMR (400 MHz, CD_2Cl_2, δ): 8.06 (d, $^3J_{H-H}$ = 8.06 Hz, naph, 1H), 8.03 (d, $^3J_{H-H}$ = 8.31 Hz, naph, 1H), 7.84 (t, $^3J_{H-H}$ = 7.55 Hz, naph, 2H), 7.63 (m, naph and Ph, 6H), 7.51 (m, Ph, 6H), 7.39 (m, Ph, 6H), 7.14 (d, Ph, $^3J_{H-H}$ = 7.81 Hz, 2H), 6.85 (s, Mes, 4H), 2.81 (d, Me, $^2J_{H-P}$ = 13.09 Hz, 3H), 2.35 (s, Me, 6H), 1.85 (s, Me, 12H) ppm. ^{31}P{^{1}H} NMR (162 MHz, CD_2Cl_2, δ): 22.4 ppm. ^{13}C NMR (100 MHz, CD_2Cl_2, δ): 150.9 (Ph), 148.0 (naph), 147.0 (Ph), 141.5 (Mes), 141.3 (Ph), 140.0 (Mes), 139.6 (naph), 138.9 (Mes), 137.6 (naph), 137.0 (Ph), 134.9 (d, Ph, J_{C-P} = 10.6 Hz), 132.9 (d, Ph, J_{C-P} = 10.9 Hz), 132.4 (d, Ph, J_{C-P} = 14.6 Hz), 131.1 (naph), 130.9 (d, Ph, J_{C-P} = 12.8 Hz), 130.1 (Ph), 129.0 (Ph), 128.3 (Mes), 128.2 (naph), 125.4 (naph), 125.2 (naph), 118.0 (d, Ph, J_{C-P} = 88.9 Hz), 114.0 (d, Ph, J_{C-P} = 90.3 Hz), 24.3 (Me), 21.5 (Me), 11.7 (d, J = 57.9 Hz, P-CH_3) ppm. The ^{11}B NMR chemical shift for **2** was not observed, perhaps because of the congested nature and the low symmetry of the molecule. Elemental analysis, calcd for $C_{53}H_{49}BPI \cdot 1H_2O$: C 72.95, H 5.89; found: C 73.19, H 6.04.

Synthesis of 1-Au. **1** (50 mg, 0.07 mmol) and Au(SMe_2)Cl (10 mg, 0.035 mmol) were dissolved in 15 mL of dry and degassed THF. The mixture was stirred overnight at ambient temperature. After the removal of the solvent in vacuo the residue was recrystallized from $CHCl_3$ and hexane, affording a colorless crystalline solid of **1-Au** (49 mg, 84%). ^{1}H NMR (400 MHz, $CDCl_3$, δ): 7.96 (d, $^3J_{H-H}$ = 7.05 Hz, naph, 4H), 7.59 (td, $^3J_{H-H}$ = 7.3 Hz, $^4J_{H-H}$ = 3.27 Hz, naph, 4H), 7.46 (m, naph and Ph, 4H), 7.35 (m, naph and Ph, 28H), 7.25 (d, $^3J_{H-H}$ = 6.29 Hz, Ph, 4H), 7.08 (d, $^3J_{H-H}$ = 7.81 Hz, Ph, 4H), 6.84 (s, Mes, 8H), 2.34 (s, Me, 12H), 1.91 (s, Me, 24H) ppm. ^{31}P{^{1}H} NMR (162 MHz, $CDCl_3$, δ): 33.5 ppm. ^{13}C NMR (100 MHz, $CDCl_3$, δ): 147.9, 147.5, 140.8, 140.2, 138.9, 138.6, 137.0, 135.5, 133.8, 133.6, 131.7, 131.5, 131.2, 129.2, 129.1, 129.0, 128.9, 128.5, 128.3, 125.6, 125.4, 24.0 (Me), 21.2 (Me) ppm. Some of the carbon chemical shifts were not observed, and the full assignment of the ^{13}C NMR spectrum could not be completed because of the low intensity and poor resolution of the ^{13}C chemical shifts caused by the poor solubility of this molecule. The ^{11}B NMR chemical shift for **1-Au** was not observed, perhaps because of the congested nature and the low symmetry of the molecule. HRMS (EI): calcd for $C_{104}H_{92}B_2P_2Cl$ $[M - Cl]^+$ 1622.6577, found 1621.6555.

Synthesis of 1-Pt. **1** (50 mg, 0.07 mmol) and Pt(SMe_2)$_2$$Cl_2$ (14 mg, 0.035 mmol) were dissolved in 15 mL of dry and degassed THF. The mixture was stirred and refluxed for 5 h. After the removal of the solvent in vacuo the residue was purified on a silica gel column (CH_2Cl_2 as the eluent), producing 49 mg of **1-Pt** as a pale yellow solid (83% yield). ^{1}H NMR (400 MHz, $CDCl_3$, δ): 7.81 (dd, $^3J_{H-H}$ = 8.08 Hz, $^4J_{H-H}$ = 3.28 Hz, naph, 4H), 7.41 (m, naph and Ph, 16H), 7.24 (m, naph and Ph, 12H), 7.12 (t, $^3J_{H-H}$ = 7.58 Hz, Ph, 8H), 7.02 (d, $^3J_{H-H}$ = 6.31 Hz, Ph, 4H), 7.93 (d, $^3J_{H-H}$ = 6.06 Hz, Ph, 4H), 6.63 (s, Mes, 8H), 2.18 (s, Me, 12H), 1.76 (s, Me, 24H) ppm. ^{31}P{^{1}H} NMR (162 MHz, $CDCl_3$, δ): 19.5 ppm (J_{P-Pt} = 1323 Hz). ^{13}C NMR (100 MHz, $CDCl_3$, δ): 147.9, 145.8, 141.4, 141.0, 140.6, 139.9, 138.2, 137.2, 135.5, 134.9, 131.0, 130.6, 130.3, 129.7, 129.2, 128.1, 127.7, 125.5, 125.3, 26.7 (Me), 21.2 (Me) ppm. Some of the carbon chemical shifts were not observed, and the full assignment of the ^{13}C NMR spectrum could not be completed because of the low intensity and poor resolution of the ^{13}C chemical shifts caused by the poor solubility of this molecule. The ^{11}B NMR chemical shift for **1-Pt** was not observed, perhaps because of the congested nature and the low symmetry of the molecule. Anal. Calcd for $C_{104}H_{92}B_2P_2PtCl_2 \cdot 0.5CH_2Cl_2$: C, 72.39; H, 5.41. Found: C, 71.97; H, 5.66.

Computational Study. The DFT calculations were performed using the Gaussian 09, revision B.01,[10] software package and the High Performance Computing Virtual Laboratory (HPCVL) at Queen's University. The ground-state geometries were fully optimized at the B3LYP[11] level using the LANL2DZ basis set for platinum and gold metal atoms and the 6-31G(d) basis set for all other atoms.[12] The initial geometric parameters in the calculations were employed from crystal structure data for geometry optimization except for compound **2** and the fluoride adducts of **1** and **2**, for which the initial geometry parameters were established by Gauss View (version 3.08). TD-DFT calculations were performed to obtain the vertical singlet and triplet excitation energies.

X-ray Crystallographic Analysis. Single crystals of **1**, **1-Au**, and **1-Pt** were mounted on glass fibers and were collected on a Bruker Apex II single-crystal X-ray diffractometer with graphite-monochromated Mo Kα radiation, operating at 50 kV and 30 mA and at 180 K. Data were processed on a PC with the aid of the Bruker SHELXTL software package (version 6.10)[13] and corrected for absorption effects. Compounds **1** and **1-Au** belong to the monoclinic crystal space groups $P2_1/c$ and $C2/c$, respectively. The crystals of **1-Pt** belong to the triclinic crystal space group $P\bar{1}$. All non-hydrogen atoms were refined anisotropically. Complete crystal structure data can be found in the Supporting Information. In the crystal lattice of **1-Au**, $CHCl_3$ solvent molecules (4 $CHCl_3$/per **1-Au**) were located and refined successfully. Two of the $CHCl_3$ solvent molecules form H bonds with the Cl ligand bound to the Au(I) atom. The crystal structure data of **1**, **1-Au**, and **1-Pt** have been deposited at the Cambridge Crystallographic Data Center (CCDC Nos. 967364−967366).

■ ASSOCIATED CONTENT

Ⓢ Supporting Information

Text, figures, tables, and CIF files giving NMR spectra for all compounds, crystal structure data for **1**, **1-Au**, and **1-Pt**, fluoride titration data, binding constant calculations, and TD-DFT computational data. This material is available free of charge via the Internet at http://pubs.acs.org.

■ AUTHOR INFORMATION

Corresponding Author

*E-mail for S.W.: wangs@chem.queensu.ca.

Notes

The authors declare no competing financial interest.

ACKNOWLEDGMENTS

We thank the Natural Sciences and Engineering Research Council for financial support and the High Performance Computing Virtual Laboratory for computing facilities. S.W. thanks the Canada Council for the Arts for the Killam Research Fellowship.

REFERENCES

(1) (a) Entwistle, C. D.; Marder, T. B. *Chem. Mater.* **2004**, *16*, 4574 and references therein. (b) Jia, W.; Feng, X.; Bai, D.; Lu, Z.; Wang, S.; Vamvounis, G. *Chem. Mater.* **2005**, *17*, 164. (c) Jia, W.; Moran, M. J.; Yuan, Y.; Lu, Z.; Wang, S. *J. Mater. Chem.* **2005**, *15*, 3326. (d) Yamaguchi, S.; Wakamiya, A. *Pure Appl. Chem.* **2006**, *78*, 1413. (e) Hudson, Z. M.; Wang, S. *Acc. Chem. Res.* **2009**, *42*, 1584. (f) Jäkle, F. *Chem. Rev.* **2010**, *110*, 3985. (g) Chen, P.; Lalancette, R. A.; Jäkle, F. *Angew. Chem., Int. Ed.* **2012**, *51*, 7994. (h) Wade, C. R.; Broomsgrove, A. E. J.; Aldridge, S.; Gabbaï, F. P. *Chem. Rev.* **2010**, *110*, 3958 and references therein. (i) Agou, T.; Sekine, M.; Kobayashi, J.; Kawashima, T. *Chem. Eur. J.* **2009**, *15*, 5056. (j) Song, K. C.; Lee, K. M.; Nghia, N. V.; Sung, W. Y.; Do, Y.; Lee, M. H. *Organometallics* **2013**, *32*, 817.

(2) (a) Liu, X.; Bai, D.; Wang, S. *Angew. Chem., Int. Ed.* **2006**, *45*, 5475. (b) Bai, D.; Liu, X.; Wang, S. *Chem. Eur. J.* **2007**, *13*, 5713. (c) Hudson, Z. M.; Liu, X.; Wang, S. *Org. Lett.* **2011**, *13*, 300. (d) Zhao, S.-B.; Wucher, P.; Hudson, Z. M.; McCormick, T. M.; Liu, X.-Y.; Wang, S. *Organometallics* **2008**, *27*, 6446.

(3) (a) Stephan, D. W. *Org. Biomol. Chem.* **2012**, *10*, 5740 and references therein. (b) Stephan, D. W.; Erker, G. *Angew. Chem., Int. Ed.* **2010**, *49*, 46. (c) Stephan, D. W. *Dalton Trans.* **2009**, 3129. (d) Voss, T.; Chen, C.; Kehr, G.; Nauha, E.; Erker, G.; Stephan, D. W. *Chem. Eur. J.* **2010**, *16*, 3005. (e) Stephan, D. W.; Greenberg, S.; Graham, T. W.; Chase, P.; Hastie, J. J.; Geier, S. J.; Farrell, J. M.; Brown, C. C.; Heiden, Z. M.; Welch, G. C.; Ullrich, M. *Inorg. Chem.* **2011**, *50*, 12338 and references therein. (f) Moret, M.-E.; Peters, J. C. *Angew. Chem., Int. Ed.* **2011**, *90*, 2063.

(4) (a) Tsurusaki, A.; Sasamori, T.; Wakamiya, A.; Yamaguchi, S.; Nagura, K.; Irle, S.; Tokitoh, N. *Angew. Chem., Int. Ed.* **2011**, *50*, 10940. (b) Li, Y.; Kang, Y.; Ko, S.; Rao, Y.; Sauriol, F.; Wang, S. *Organometallics* **2013**, *32*, 3063. (c) Beckmann, J.; Hupf, E.; Lork, E.; Mebs, S. *Inorg. Chem.* **2013**, *52*, 11881. (d) Bontemps, S.; Devillard, M.; Mallet-Ladeira, S.; Bouhadir, G.; Miqueu, K.; Bourissou, D. *Inorg. Chem.* **2013**, *52*, 4714.

(5) (a) Lee, M. H.; Agou, T.; Kobayashi, J.; Kawashima, T.; Gabbaï, F. P. *Chem. Commun.* **2007**, 1133. (b) Hudnall, T. W.; Kim, Y.; Bebbington, M. W. P.; Bourissou, D.; Gabbaï, F. P. *J. Am. Chem. Soc.* **2008**, *130*, 10890.

(6) (a) Gimeno, M. C.; Laguna, A. *Chem. Rev.* **1997**, *97*, 511. (b) Rigamonti, L.; Manassero, C.; Rusconi, M.; Manassero, M.; Pasini, A. *Dalton Trans.* **2009**, 1206.

(7) (a) Bowmaker, G. A.; Dyason, J. C.; Healy, P. C.; Engelhardt, L. M.; Pakawatchai, C.; White, A. H. J. *Dalton Trans.* **1987**, 1089. (b) Baenziger, N. C.; Dittemore, K. M.; Doyle, J. R. *Inorg. Chem.* **1974**, *13*, 805. (c) Khan, M. N. I.; Staples, R. J.; King, C.; Fackler, J. P., Jr.; Winpenny, R. E. P. *Inorg. Chem.* **1993**, *32*, 5800. (d) Wade, C. R.; Lin, T.-P.; Nelson, R. C.; Mader, E. A.; Miller, J. T.; Gabbaï. *J. Am. Chem. Soc.* **2011**, *133*, 8948.

(8) Marsh, W. C.; Trotter, J. *J. Chem. Soc. A* **1971**, 1482.

(9) (a) Kim, Y.; Gabbaï, F. P. *J. Am. Chem. Soc.* **2009**, *131*, 3363. (b) Hudnall, T. W.; Chiu, C. W.; Gabbaï, F. P. *Acc. Chem. Res.* **2009**, *42*, 388. (c) Broomsgrove, A. E. J.; A. Addy, D.; Di Paolo, A.; Morgan, I. R.; Bresner, C.; Chislett, V.; Fallis, I. A.; Thompson, A. L.; Vidovic, D.; Aldridge, S. *Inorg. Chem.* **2010**, *49*, 157. (d) Kim, Y.; Huh, H.-S.; Lee, M. H.; Lenov, I. L.; Zhao, H.; Gabbaï, F. P. *Chem. Eur. J.* **2011**, *17*, 2057. (e) Zhao, H.; Leamer, L. A.; Gabbaï, F. P. *Dalton Trans.* **2013**, *42*, 8164 and references therein.

(10) Frisch, M. J.; Trucks, G. W.; Schlegel, H. B.; Scuseria, G. E.; Robb, M. A.; Cheeseman, J. R.; Scalmani, G.; Barone, V.; Mennucci, B.; Petersson, G. A.; Nakatsuji, H.; Caricato, M.; Li, X.; Hratchian, H. P.; Izmaylov, A. F.; Bloino, J.; Zheng, G.; Sonnenberg, J. L.; Hada, M.; Ehara, M.; Toyota, K.; Fukuda, R.; Hasegawa, J.; Ishida, M.; Nakajima, T.; Honda, Y.; Kitao, O.; Nakai, H.; Vreven, T.; Montgomery, J. A., Jr.; Peralta, J. E.; Ogliaro, F.; Bearpark, M.; Heyd, J. J.; Brothers, E.; Kudin, K. N.; Staroverov, V. N.; Keith, T.; Kobayashi, R.; Normand, J.; Raghavachari, K.; Rendell, A.; Burant, J. C.; Iyengar, S. S.; Tomasi, J.; Cossi, M.; N. Rega, N.; Millam, J. M.; Klene, M.; Knox, J. E.; Cross, J. B.; Bakken, V.; Adamo, C.; Jaramillo, J.; Gomperts, R.; Stratmann, R. E.; Yazyev, O.; Austin, A. J.; Cammi, R.; Pomelli, C.; Ochterski, J. W.; Martin, R. L.; Morokuma, K.; Zakrzewski, V. G.; Voth, G. A.; Salvador, P.; Dannenberg, J. J.; Dapprich, S.; Daniels, A. D.; Farkas, O.; Foresman, J. B.; Ortiz, J. V.; Cioslowski, J.; Fox, D. J. *Gaussian09, revision B.01*; Gaussian, Inc., Wallingford, CT, 2010.

(11) (a) Lee, C.; Yang, W.; Parr, R. G. *Phys. Rev. B* **1988**, *37*, 785−789. (b) Becke, A. D. *J. Chem. Phys.* **1993**, *98*, 5648−5652.

(12) Hay, P. J. *J. Phys. Chem. A* **2002**, *106*, 1634.

(13) *SHELXTL Version 6.14*; Bruker AXS, Madison, WI, 2000−2003.